JOURNAL OF INTEGRAL EQUATIONS
AND APPLICATIONS
Volume 19, Number 3, Fall 2007

NONLINEAR INTEGRAL EQUATION METHODS FOR THE RECONSTRUCTION OF AN ACOUSTICALLY SOUND-SOFT OBSTACLE

OLHA IVANYSHYN AND TOMAS JOHANSSON

ABSTRACT. The problem considered is that of determining the shape of a planar acoustically sound-soft obstacle from knowledge of the far-field pattern for one time-harmonic incident field. Two methods, which are based on the solution of a pair of integral equations representing the incoming wave and the far-field pattern, respectively, are proposed and investigated for finding the unknown boundary. Numerical results are included which show that the methods give accurate numerical approximations in relatively few iterations.

1. Introduction. In applications such as medical imaging, nondestructive testing, prospecting for oil and gas, and radar and sonar obstacle detection, a typical problem is to find the shape of an unknown obstacle using information from the influence that the obstacle has on propagating waves. This situation can be modeled mathematically as a so-called inverse obstacle scattering problem. In this paper we consider, for simplicity, an inverse scattering problem where the shape of a planar acoustically sound-soft obstacle is to be determined from measurements of the far field pattern (the asymptotic behavior of the scattered field at large distances from the obstacle) for one time-harmonic incident field with wave number $k > 0$. The ideas presented can, in principle, be applied to other types of inverse scattering problems for time-harmonic waves, e.g., sound hard and impedance boundary conditions. The difficulty found when trying to solve for the shape of an obstacle is due to the fact that the problem is both nonlinear and severely ill-posed in the Hadamard sense [**7**].

Keywords and phrases. Far field pattern, ill-posed, inverse scattering, Newton method, Tikhonov regularization, sound-soft.

The first author acknowledges the support of her work by the Graduiertenkolleg 1023 as well as support from the Computational Fluid Dynamics Centre at the University of Leeds via EST, Marie Curie funding. The second author acknowledges support from the Wenner-Gren foundations.

Received by the editors on July 17, 2006, and in revised form on October 24, 2006.

Several different iterative methods exist to approximate solutions of the inverse scattering problem under consideration. One group of methods decomposes it into two parts, a linear ill-posed equation for finding the scattered wave from the far field and then a nonlinear well-posed one to find the boundary, see for example Colton and Monk [**3, 4**], Kirsch et al. [**13**] and Potthast [**18**]. Another group of methods recasts the obstacle reconstruction in the form of a nonlinear operator equation and uses iterative Newton type methods to find approximations to the nonlinear equation, see Kirsch [**11**]. These methods often require the solution of the direct scattering problem at each step. Alternative approaches which avoid solving the direct problem have been considered by Kress and Rundell [**14**] and Kress and Serranho [**15**], and whilst these involve a linearization they do not require the solution of a sequence of direct problems. All of the above-mentioned procedures can, in principle, work with knowledge of the far field pattern for only one incoming wave, although in most numerical examples several different incoming waves are used to acquire accurate approximations. Sampling methods such as the linear sampling method introduced by Colton and Kirsch [**1**], the point-source method by Potthast [**18**], the factorization method by Kirsch [**12**] and the probe method by Ikehata [**8**], require knowledge of the far field pattern for a large number of different directions of the incoming wave.

Recently a method, first proposed in [**20**], for the reconstruction of the shape of a planar acoustically sound-soft obstacle from measurements of the far-field pattern for one incident field was analyzed and implemented, see Johansson and Sleeman [**10**]. Independently, Ivanyshyn and Kress [**9**] have proposed a related approach. Both these methods are based on the boundary integral equations for the incident field and the far-field pattern, respectively, (these equations can be found in Section 3.1), together with the assumption that the boundary curve of the obstacle has a polar representation. The numerical examples presented in [**9, 10**] show that these algorithms give accurate numerical approximations, even on the shadow side, in relatively few iterations.

In this paper, we extend the methods [**9, 10**] to more general boundary curves and make numerical comparisons between them. The precise formulation of the inverse scattering problem under study and some of its properties are given in Section 2. The two procedures are then presented in Section 3. We also discuss the relationship

between these algorithms and the classical approach in [**2**] which uses the boundary to far field operator, see the remark at the end of the paper. Numerical analysis and discussions of the iterative procedures are presented in Section 4. These numerical experiments indicate that both methods give accurate numerical approximations in few iterations.

2. The inverse scattering problem. Let the planar obstacle be represented by a bounded simply connected domain D in $\mathbf{R}^2$ with C^2 boundary Γ. The outward unit normal to Γ is denoted by ν and, as usual, Δ denotes the Laplace operator. The space-dependent part of the incoming time-harmonic wave is $u^i(x) = e^{ikx\cdot d}$, where the wave number k is a real positive number and $d = (\cos\varphi_0, \sin\varphi_0)$ is the direction of the incoming wave. We denote the scattered field by u^s.

The direct scattering problem for a sound-soft obstacle is then: given the incident field u^i, find the total field $u = u^i + u^s$ such that u solves the Helmholtz equation in the exterior of the obstacle and is zero on the boundary, i.e.,

$$\begin{cases} \Delta u + k^2 u &= 0 \ \text{ in } \ \mathbf{R}^2 \setminus \overline{D}, \\ u &= 0 \ \text{ on } \ \Gamma, \end{cases} \tag{2.1}$$

and the scattered wave u^s satisfies the Sommerfeld radiation condition

$$\lim_{r\to\infty} r^{1/2}\left(\frac{\partial u^s}{\partial r} - iku^s\right) = 0, \text{ where } r = |x|,$$

uniformly in all directions. This condition ensures uniqueness of the solution to the scattering problem and guarantees that the scattered wave is outgoing. Since the boundary Γ is smooth there exists a unique solution $u \in C^2(\mathbf{R}^2 \setminus \overline{D}) \cap C(\mathbf{R}^2 \setminus D)$, see Theorem 3.9 in Colton and Kress [**2**]. Moreover, one can show the following asymptotic behavior of the scattered field

$$u^s(x) = \frac{e^{ik|x|}}{|x|^{1/2}}\Big(u_\infty(x/|x|) + O(|x|^{-1})\Big), \quad |x| \to \infty,$$

where u_∞ is the far field pattern or the scattering amplitude and is defined on the unit circle in $\mathbf{R}^2$.

Given measurements of the far field pattern for one incoming wave it is natural to consider the question of finding the obstacle which

produces such a far field. This is the inverse problem that we will consider. It is both nonlinear and severely ill-posed, thus difficult to solve. We assume that the data is chosen so that there exists a solution and according to results of Colton and Sleeman [**5**] we also have uniqueness:

Lemma 2.1. *Let D_1 and D_2 be two planar scatterers contained in a disk of radius R such that $kR < C$, where C is the smallest positive zero of the Bessel function J_0 (approximately 2.4048). If the corresponding far field patterns coincide for one incident field with wave number k, then D_1 and D_2 coincide.*

Before ending this section, we recall, see [**2**, Section 3], that one can choose a density $\psi := \partial u/\partial\nu|_\Gamma$ such that

$$u^s(x) = -\frac{i}{4}\int_\Gamma H_0^{(1)}(k|x-y|)\,\psi(y)\,dS(y), \quad \text{for } x \in \Gamma, \tag{2.2}$$

and

$$u_\infty(\hat{x}) = \gamma\int_\Gamma e^{-ik\hat{x}\cdot y}\,\psi(y)\,dS(y), \quad \text{for } \hat{x} = x/|x|, \tag{2.3}$$

where $\gamma = -e^{i\pi/4}/\sqrt{8\pi k}$ and $H_0^{(1)}$ is the Hankel function of the first kind of order zero (apart from a constant it is the fundamental solution to the Helmholtz equation in $\mathbf{R}^2$).

3. Two iterative methods for the inverse scattering problem. We assume that the boundary Γ has a C^2-smooth and 2π-periodic representation

$$z(t) = (z_1(t), z_2(t)), \quad \text{for } t \in [0, 2\pi], \tag{3.1}$$

with positive orientation and $|z'(t)| > 0$, where $t \in [0, 2\pi]$.

3.1 *Boundary integral equations for u^i and u_∞.* Here, we give parameterized boundary integral operators representing the scattered field and its far field pattern. Put

$$\Phi(t,\tau) = \frac{i}{4}H_0^{(1)}(kr(t,\tau)),$$

where $r(t,\tau) = |z(t) - z(\tau)|$, and let $\varphi(t) = \psi(z(t))|z'(t)|$. Furthermore, let $S : L^2([0,2\pi]) \to L^2([0,2\pi])$ be the parameterized single-layer integral operator

$$(S\varphi)(t) = \int_0^{2\pi} \Phi(t,\tau)\,\varphi(\tau)\,d\tau, \quad \text{for } t \in [0,2\pi]. \tag{3.2}$$

Similarly, let $S_\infty : L^2([0,2\pi]) \to L^2([0,2\pi])$ be the operator

$$(S_\infty\varphi)(\theta) = \gamma \int_0^{2\pi} e^{-ikx_\infty(\theta)\cdot z(\tau)}\,\varphi(\tau)\,d\tau, \quad \text{for } \theta \in [0,2\pi], \tag{3.3}$$

where $x_\infty(\theta) = (\cos\theta, \sin\theta)$ is a parameterization of the unit circle in $\mathbf{R}^2$. To indicate the dependence on the boundary Γ, we write $S(z,\varphi)$ and $S_\infty(z,\varphi)$ instead of $S\varphi$ and $S_\infty\varphi$, respectively.

Using the sound-soft boundary condition in (2.1) together with the knowledge of the far field pattern we obtain a system of two integral equations

$$S(z,\varphi)(t) = u^i(z(t)), \quad \text{for } t \in [0,2\pi], \tag{3.4}$$

and

$$S_\infty(z,\varphi)(\theta) = u_\infty(\theta), \quad \text{for } \theta \in [0,2\pi]. \tag{3.5}$$

The methods for the reconstruction of the shape of the obstacle presented in the next two subsections are based on this system.

3.2 *Method* A. The method presented here was considered in [**10**] for boundaries Γ given by a polar representation. An extension of the method to a more general class of boundary curves is described below.

To start the procedure, we make an initial guess of the unknown boundary curve Γ of the obstacle. This guess is denoted by Γ_0 and is parameterized by v_0. Then (3.4) with $z = v_0$ is a Fredholm integral equation of the first kind with a logarithmic singularity for the determination of the density φ. Such an integral equation is well studied and a solution can, for example, be obtained using the Nyström method described below. Once this density is found, one substitutes it into the nonlinear integral equation (3.5) to obtain a new approximation

v_1 to Γ. This integral equation can be solved by a variety of methods, for example the Levenberg-Marquardt type method presented in [**6**]. The iterative procedure can then be repeated until the desired level of approximation is obtained. To summarize:

1. Choose a (closed) curve Γ_0 described as $z = v_0$.

2. Knowing the curve Γ_{m-1} parameterized by $z = v_{m-1}$, where $m \geq 1$ and using (3.4), we calculate a new density $\varphi = \varphi_{m-1}$.

3. The next approximation to Γ will be Γ_m: $z = v_m$, where z is calculated from (3.5) with $\varphi = \varphi_{m-1}$.

The procedure then continues by iterating on the last two steps until a suitable stopping criteria is satisfied.

For the numerical implementation of this procedure, let us first describe how one can solve (3.4) for the density φ given a parameterization z. The kernel Φ has a logarithmic singularity and can be written as

$$\Phi(t,\tau) = \Phi_1(t,\tau)\ln\left(4\sin^2\frac{t-\tau}{2}\right) + \Phi_2(t,\tau),$$

with smooth functions Φ_1 and Φ_2. For the numerical solution of (3.4) it is effective to apply a Nyström type method using a trigonometrical approximation $\widetilde{\varphi}$ of the density φ, where

$$\widetilde{\varphi}(t) = \frac{a_0}{2} + \sum_{m=1}^{n-1}(a_m\cos mt + b_m\sin mt) + \frac{a_n}{2}\cos nt, \tag{3.6}$$

together with the trapezoidal rule and logarithmic singularity quadrature on the mesh-points $(\pi/n)j$, $j = 0, 1, \ldots, 2n$, see [**16**] for the details.

Let $H^p([0,2\pi])$ for $p \geq 1$ be the Sobolev space of 2π-periodic functions on the interval $[0,2\pi]$, i.e., the space of 2π-periodic functions φ with the property

$$\sum_{m=-\infty}^{\infty}(1+m^2)^p|c_m|^2 < \infty,$$

where the c_m are the Fourier coefficients of φ. According to [**16**], we have the following

Lemma 3.1. *Assume that $\varphi \in H^p([0,2\pi])$, where $p > 3/2$, is a solution to (3.4). Then, for a sufficiently large integer $n > 0$, the*

corresponding discretized equations obtained from the Nyström method *have a unique solution* φ_n *of the form* (3.6) *and*

$$\|\varphi - \varphi_n\|_{H^q([0,2\pi])} \le C \left(\frac{\pi}{n}\right)^{p-q} \|\varphi\|_{H^p([0,2\pi])}, \quad \text{for } 1 \le q \le p. \tag{3.7}$$

Note that for infinitely differentiable boundaries and data, the convergence rate of the Nyström method is faster than any power of the step length.

Now we describe how to solve equation (3.5) for the unknown parameterization $z(t)$ for a given density φ. Let $C^\ell[0,2\pi]$, where $0 \le \ell \le 2$, be the space of 2π-periodic and ℓ times differentiable functions on $[0,2\pi]$, $(C = C^0)$. By $B(C[0,2\pi], C[0,2\pi])$, we denote the space of bounded linear operators on $C[0,2\pi]$. From Theorem 3 in [**17**], we have

Lemma 3.2. *The mapping* $C^2[0,2\pi] \to B(C[0,2\pi], C[0,2\pi])$ *given by* $z \mapsto S_\infty(z,\cdot)$ *is Fréchet differentiable with derivative*

$$(S'_\infty[z,\varphi]h)(\theta) = -ik\gamma \int_0^{2\pi} e^{-ikx_\infty(\theta)\cdot z(\tau)} \varphi(\tau)\, x_\infty(\theta) \cdot h(\tau)\, d\tau, \quad \theta \in [0,2\pi]. \tag{3.8}$$

Given a density φ and a current approximation $z(t) = v_{m-1}(t)$, we find v_m using (3.5) as follows

$$v_m = v_{m-1} - \rho\, ((S'_\infty)^* S'_\infty + \lambda_m I_p)^{-1} (S'_\infty)^* (S_\infty(v_{m-1},\varphi) - u_\infty), \tag{3.9}$$

where $S'_\infty = S'_\infty[v_{m-1},\varphi]$ and $(S'_\infty)^*$ stands for the L^2 adjoint of S'_∞. So the new approximation v_m is obtained from a scaled Newton step with Tikhonov regularization and H^p penalty term, where $p \ge 0$. The scaling factor $\rho \ge 0$ is fixed throughout the iterations and according to [**6**] the parameter λ_m can be chosen as

$$\lambda_m = \|u_\infty - S_\infty(v_{m-1},\varphi)\|_{L^2}^\mu, \quad \mu > 0. \tag{3.10}$$

The integrals in (3.9) will be discretized using the trapezoidal rule.

3.3 *Method* B. Here, we give an extension to more general parameterizations of the method introduced in [**9**]. This method involves the full linearization of the system of integral equations (3.4)–(3.5) with respect to both the boundary parameterization and the density. After linearization we obtain

$$\begin{cases} S(z,\varphi) + S(z,\zeta) + S'[z,\varphi]h = u^i(z) + u^{i\,\prime}[z]h, \\ S_\infty(z,\varphi) + S_\infty(z,\zeta) + S'_\infty[z,\varphi]h = u_\infty. \end{cases} \tag{3.11}$$

Here

$$(S'[z,\varphi]h)(t) = \frac{ik}{4}\int_0^{2\pi} H_0^{(1)\,\prime}(kr(t,\tau)) \times \frac{[z(t)-z(\tau)]\cdot[h(t)-h(\tau)]}{r(t,\tau)}\,\varphi(\tau)\,d\tau, \quad t\in[0,2\pi]$$

with $r(t,\tau)=|z(t)-z(\tau)|$, $u^{i\,\prime}[z]h = iku^i(d\cdot h)$ and $S'_\infty[z,\varphi]h$ given by Lemma 3.2. For simplicity we rewrite the system (3.11) in the form

$$A\begin{pmatrix}\zeta\\ h\end{pmatrix} = f, \tag{3.12}$$

where

$$A = \begin{pmatrix} S(z,\cdot\,) & S'[z,\varphi] - u^{i\,\prime}[z] \\ S_\infty(z,\cdot\,) & S'_\infty[z,\varphi] \end{pmatrix} \text{ and } f = \begin{pmatrix} u^i(z) - S(z,\varphi) \\ u_\infty - S_\infty(z,\varphi) \end{pmatrix}.$$

To start the procedure we make an initial guess of the unknown boundary Γ parameterized by $v_0(t)$. Then the density φ_0 is found from (3.4). Solving the linear system (3.12) with $\varphi=\varphi_0$ and $z=v_0$ gives the corrections ζ and h from which we update the density and the boundary as $\varphi_1=\varphi_0+\zeta$ and $v_1=v_0+h$, respectively.

To summarize:

1. Choose a (closed) curve Γ_0 parameterized by $z(t)=v_0(t)$.

2. Find $\varphi=\varphi_0$ from (3.4).

3. Knowing the current approximation (φ_{m-1}, v_{m-1}), where $m\geq 1$, from the linear system (3.12) we find a correction (ζ, h) and update the approximation as $\varphi_m=\varphi_{m-1}+\zeta$ and $v_m=v_{m-1}+h$.

Until a suitable stopping criteria is satisfied the procedure continues by repeating the last step.

The ill-posedness of the inverse problem requires regularization to be incorporated. We will use the well-established Tikhonov regularization, so instead of (3.12) the following system will be solved

$$(A^* \; A + \lambda_m \widetilde{I}_p) \begin{pmatrix} \zeta \\ h \end{pmatrix} = A^* f$$

with $L^2 \times H^p$ penalty term where

$$\widetilde{I}_p = \begin{pmatrix} I_0 & 0 \\ 0 & I_p \end{pmatrix} \text{ and } \lambda_m = \left(\frac{2}{3}\right)^m \begin{pmatrix} \alpha \\ \beta \end{pmatrix}. \tag{3.13}$$

Discretization is carried out as in the previous section; for further details, see [**9**].

4. Numerical examples. In this section we carry out numerical investigations of the two methods presented in Section 3. Reconstructions of three different types of obstacles will be considered, from exact as well as noisy data, for various initial guesses and incoming waves. The corresponding far field pattern is numerically generated at 64 points equally distributed around the unit circle by solving the integral equations (3.4) and (3.5) with the number of collocation points doubled in order to avoid the "inverse crime." Furthermore, we obtained similar far field patterns by using coupled variants of these integral equations. Noisy data u_∞^δ is constructed in the following way

$$u_\infty^\delta = u_\infty + \delta \frac{\|u_\infty\|_{L^2}}{\|\eta\|_{L^2}} \eta, \tag{4.1}$$

where $\eta = \eta_1 + i\eta_2$ and η_1 and η_2 are normally distributed random variables and δ is the relative noise level. For simplicity the wave number k is set equal to 1 and the initial guess is taken to be a circle indicated by dotted lines in the figures throughout the examples. We also tried different shapes for the initial guess, for example an ellipse, but changing the guess does not affect the procedure as long as this guess is not too small or too large. In the first two examples we assume that the boundary Γ of the obstacle has a polar parameterization, e.g.,

$$z(t) = r(t)(\cos t, \sin t), \quad t \in [0, 2\pi] \tag{4.2}$$

which is not the case in the third example where instead the obstacle has the general parameterization (3.1). We display the analytical boundary curve as a solid line in all of the figures.

TABLE 1. Results for exact data, pinched ellipse.

Initial radius	Rel. error level (%)	Method A		Method B	
		reg. par. μ	number of iterations	reg. par. α β	number of iterations
0.1	5	1	10	10^{-3} 10^{0}	11
	1	1	25	10^{-3} 10^{0}	38
1.2	5	4	8	10^{-9} 10^{-7}	3
	1	4	11	10^{-9} 10^{-7}	8
2	5	2	16	10^{-3} 10^{-1}	8
	1	2	22	10^{-3} 10^{-1}	34

Example 1. We wish to reconstruct a pinched ellipse given by the equation

$$z(t) = \frac{3}{2}\left(\frac{1}{4}\cos^2 t + \sin^2 t\right)^{1/2}(\cos t, \sin t), \quad t \in [0, 2\pi].$$

Since the radial function r in (4.2) is 2π-periodic it is natural to approximate it by a trigonometrical polynomial

$$\widetilde{r}(t) = a_0 + \sum_{m=1}^{N_T}(a_m \cos mt + b_m \sin mt), \quad t \in [0, 2\pi]. \tag{4.3}$$

In the discretized versions of methods A and B the coefficients in (4.3) are constructed for the pinched ellipse. In Table 1 we present the number of iterations needed for methods A and B to obtain 5% and 1% relative L^2 error in the reconstruction for different initial guesses. These guesses are circles centered at the origin with radii as stated in the table, the direction of the incoming wave is $(\cos \pi/3, \sin \pi/3)$ and $N_T = 12$ in (4.3). For method A the scaling factor in (3.9) is $\rho = 0.8$ and μ in (3.10) is given in the table, as well as the parameters α and β

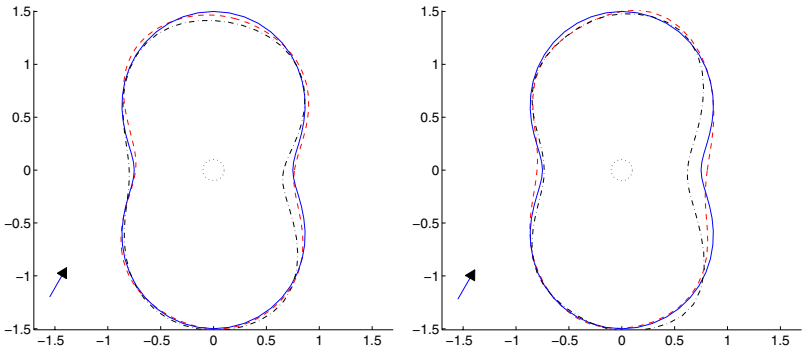

FIGURE 1. Reconstruction of a pinched ellipse noisy data.
a) Method A; b) Method B.

in (3.13) for method B. Throughout this example $p = 1$ in (3.9), (3.13), i.e., an H^1 penalty term is used in method A and an $L^2 \times H^1$ penalty term is used in method B.

From Table 1 we conclude that method B gives a reasonable reconstruction in fewer iterations than method A; on the other hand, to decrease the relative error from 5% to 1% method A requires less iterations in general.

As an initial guess the smallest and largest radii of circles with center at the origin which give accurate approximations were 0.001 and 2.4 for Method A and 0.001 and 2.9 for Method B, respectively. The direction of the incoming wave can be changed and the methods produce similar results.

For further investigations 10 different sets of perturbed far field data in the form (4.1) with relative noise level $\delta = 0.03$ were generated. We used these data sets for both methods A and B and present in Table 2 the best, respectively, average relative L^2 error between the reconstruction and exact curve and the mean number of iterations. The parameters were kept fixed for different incident directions and initial guesses and assumed the values $\rho = 1$, $\mu = 4$ and $\alpha = 10^{-3}$, $\beta = 1$ for the methods A and B, respectively. Initial guesses were chosen as in the case of exact data.

In Figure 1 the reconstructions for the incoming wave direction $(\cos \pi/3, \sin \pi/3)$ with initial guess a circle of radius 0.1 are shown, where the dashed lines and dash-dot lines are the approximations with the minimal and maximal relative error from Table 2.

TABLE 2. Results for noisy data, pinched ellipse.

Initial radius	Incident direction	Method A			Method B		
		rel. error (best)	rel. error (mean)	iterations (mean)	rel. error (best)	rel. error (mean)	iterations (mean)
0.1	0	0.0207	0.0397	31	0.0246	0.0476	13
	$\pi/3$	0.0218	0.0354	24	0.0272	0.0476	13
	$\pi/2$	0.0153	0.0251	23	0.0246	0.0332	12
1.2	0	0.0224	0.0399	11	0.0375	0.0540	12
	$\pi/3$	0.0243	0.0360	11	0.0189	0.0335	11
	$\pi/2$	0.0152	0.0243	9	0.0242	0.0371	11
2	0	0.0152	0.0243	9	0.0502	0.0674	13
	$\pi/3$	0.0217	0.0358	16	0.0245	0.0382	11
	$\pi/2$	0.0169	0.0266	16	0.0216	0.0374	11

From Table 2 it can be seen that method B in general requires less iterations but method A is more accurate. If the procedures are continued beyond the iteration values given in the table, the relative errors begin to magnify since the regularization parameters in (3.10) and (3.13) are decreasing.

Example 2. The boundary of the obstacle to be reconstructed in this example has the nonsymmetrical shape

$$z(t) = \left(\frac{1 + 0.9\cos t + 0.1\sin 2t}{1 + 0.75\cos t}\right)(\cos t, \sin t), \quad t \in [0, 2\pi].$$

To obtain a faster reconstruction (with less unknowns in the procedures) of the indented part of this obstacle, see Figure 3, we approximate the function r in (4.2) by radial basis functions which have a more localized behavior than (4.3), i.e.,

$$\widetilde{r}(t) = \sum_{m=1}^{N_R} a_m e^{-\gamma \sin^2(t-t_m)/2}, \quad t \in [0, 2\pi], \tag{4.4}$$

where $t_m = 2\pi m/N_R$ for $m = 1, 2, \ldots, N_R$ and $\gamma \approx N_R$. This basis function, for $N_R = 9$ and $\gamma = N_R$, is shown in Figure 2.

To compare the reconstructions for exact data obtained with trigonometrical and radial basis interpolations, we choose $N_T = 4$ in (4.3) and

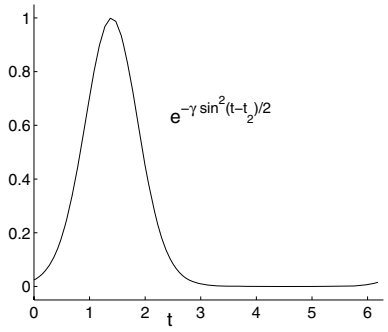

FIGURE 2. A radial basis function.

$N_R = 9$ in (4.4), that is, we maintain the same number of unknown coefficients. In Figure 3 a) the reconstructions produced by method A after 20 iterations with parameters $\rho = 0.9$ in (3.9) and $\mu = 3$ in (3.10) with L^2 penalty term, are presented. Correspondingly, in Figure 3 b) we see the results generated by method B after 10 iterations and parameters $\alpha = 10^{-8}$, $\beta = 10^{-7}$, with $L^2 \times L^2$ penalty term. In both figures the initial guess is a circle of radius 0.8, the dash–dot and dashed lines are the reconstructions with trigonometrical and radial basis interpolations, respectively. By the arrow we denote the direction of the incoming incident wave.

With the same number of unknowns both methods produce a more accurate reconstruction using the radial basis functions. However if we

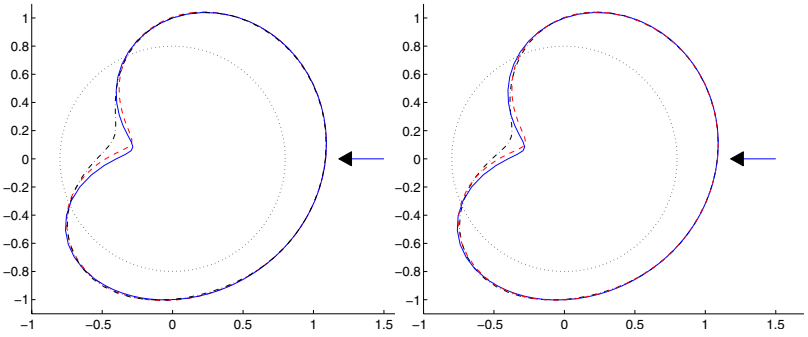

FIGURE 3. Reconstruction of an apple shaped contour, exact data.
a) Method A; b) Method B.

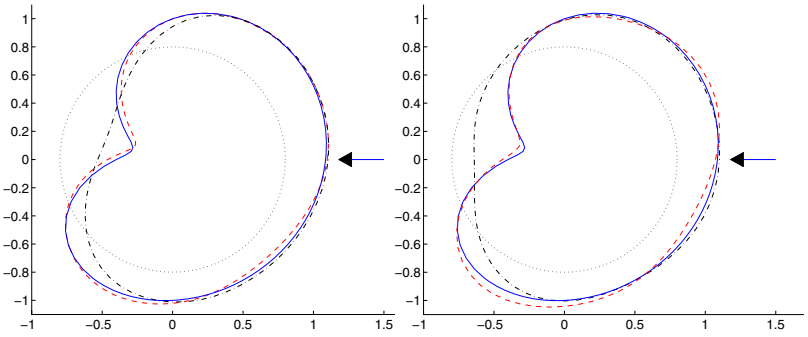

FIGURE 4. Reconstruction of an apple shaped domain, noisy data.
a) Method A; b) Method B.

increase the degree of approximation the results become similar for both the trigonometrical and radial basis interpolations. Note also that the shadow side of the contour, containing the indented part, is accurately reconstructed.

As in the first example, ten data sets of perturbed far field data with 3% noise level are generated. In Figure 4 the reconstructions using radial basis interpolation, with the least (dashed line) and the highest (dash–dot line) relative L^2 error, are presented. The same regularization parameters as in the case of exact data were used for method A but for method B they were changed to $\alpha = 0.1$, $\beta = 1$. The error levels and the number of iterations for the procedures are presented in Table 3.

TABLE 3. Noisy data, radial basis approximation.

	Method A		Method B	
	rel. error	iterations	rel. error	iterations
least	0.0311	8	0.0325	14
average	0.0618	12	0.0694	16

Example 3. Finally, we attempt to reconstruct a boundary curve with the parameterization

$$z(t) = (\cos t + 0.65\cos 2t - 0.65, 1.5\sin t), \quad t \in [0, 2\pi].$$

In [**9**] the reconstructions of this curve using the polar representation (4.2) are presented. To improve the accuracy it is natural to use the

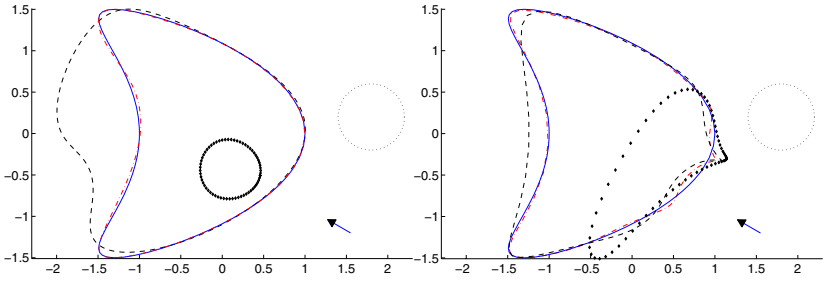

FIGURE 5. Reconstruction of a kite contour, exact data.
a) Method A; b) Method B.

more general parameterization (3.1). Each of the functions z_1, z_2 in (3.1) are approximated by the trigonometrical polynomials (4.3) with $N_T = 7$. We investigate how the location of the initial guess and the direction of the incoming wave influence the procedures.

We begin by choosing the direction of the incoming wave as $(\cos 5\pi/6, \sin 5\pi/6)$ and the initial guess a circle of radius 0.4 with the center located outside of the obstacle. To obtain a faster reconstruction the parameter choice rule at each iteration step for method A was changed from (3.10) to $\lambda_m = 40 \cdot 2^{-0.5m}$ (m is the iteration index) with the scaling factor $\rho = 1$. For method B the parameters are $\alpha = 0.1$, $\beta = 1$. Moreover, for both procedures, to acquire a smoother reconstruction, we use $p = 2$ in (3.9) and (3.13).

The thick dotted line in Figure 5 a) and b) represents the boundary curve obtained after 5 iterations, the dashed line after 25 iterations and the dash–dot line after 50 iterations for exact data. As we can see from this figure, in method A, the initial guess is first moved almost unchanged towards the center of the obstacle. Then the illuminated region is reconstructed and finally the shadow is found. This is not the case in method B, where the illuminated region is found almost directly and then the shadow region is reached. We could move the initial guess further to the right but not beyond the disk mentioned in Lemma 2.1.

We then placed the initial guess inside the obstacle but far from the center, see Figure 6. The notations and parameters are the same as in the previous figure. We point out that, if the initial guess is located in the shadow region outside the obstacle, then inaccurate reconstructions were obtained.

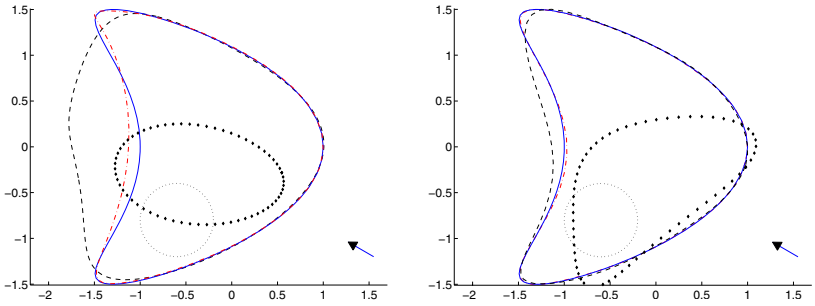

FIGURE 6. Reconstruction of a kite contour, exact data.
a) Method A; b) Method B.

Next, the direction of the incoming wave is changed to $(1, 0)$ and the initial guess is moved towards the indented part, see Figure 7. Again, the methods produced reconstructions in the same way as described-above but fewer iterations are needed. The notations are as in the previous figures except that the dashed lines denote the reconstruction after 15 iterations and the dash–dot lines after 30 iterations.

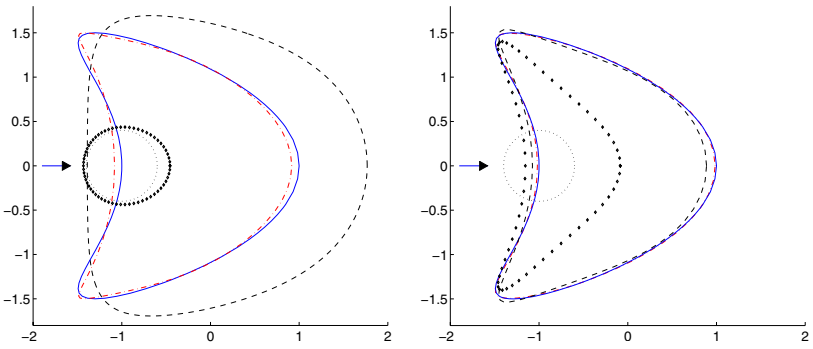

FIGURE 7. Reconstruction of a kite contour, exact data.
a) Method A; b) Method B.

The initial guess for this direction can also be placed outside of the obstacle provided that it is not located too far into the shadow region. For the situation illustrated in Figure 8 the regularization parameter α was changed to 0.01 for method B whilst the other parameters remained the same for both methods.

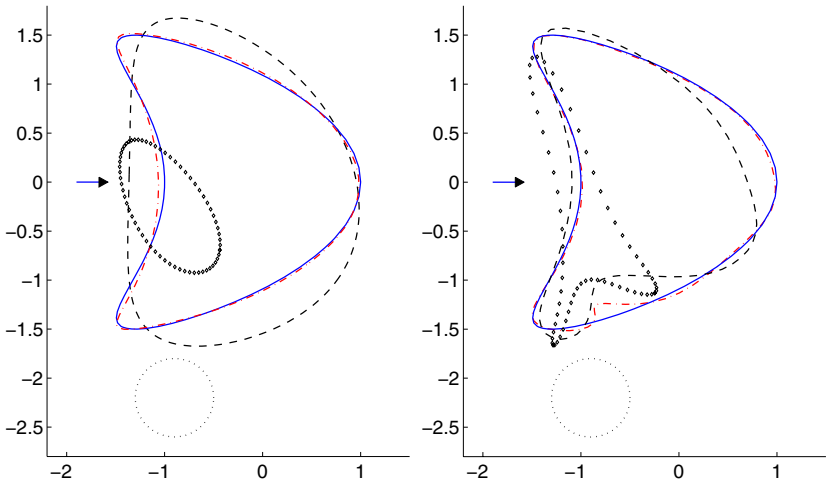

FIGURE 8. Reconstruction of a kite contour, exact data.
a) Method A; b) Method B.

Finally, ten sets of noisy data were generated with the noise level $\delta = 0.03$ in (4.1). The iterations were terminated once the term

$$e_m = \frac{1}{64}\left(\sum_{j=0}^{63} \min_{x\in\Gamma} |x - x_j^{(m)}| + \big||\Gamma| - |\Gamma_m|\big| \right) \tag{4.5}$$

began to increase. In (4.5) the boundary curve Γ_m is the reconstruction obtained at the mth step, $x_j^{(m)}$ are the corresponding collocation points on this curve and $|\Gamma_m|$ denotes the boundary length.

The dash–dot line in Figure 9 is the least accurate reconstruction using e_m as a stopping criteria whilst the dashed line is the best one. The actual values are presented in Table 4. The parameters of the procedures are unchanged from Figure 8.

TABLE 4. Noisy data, kite reconstruction.

	Method A		Method B	
	e_m	iterations	e_m	iterations
least	0.0880	29	0.0924	18
highest	0.1684	29	0.1467	17

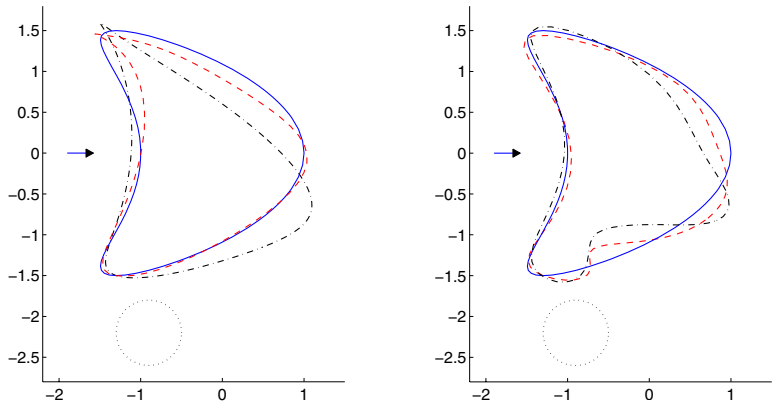

FIGURE 9. Reconstruction of a kite contour, noisy data.
a) Method A; b) Method B.

Remark. Formally, if k^2 is not an interior eigenvalue for the negative Laplacian, given a parameterization $z(t)$ one can uniquely solve (3.4) for the density φ, i.e., the operator $S_0 u^i(z) = S^{-1}(z,\cdot)u^i(z)$ is well defined. Using this expression in (3.5) we obtain the boundary to far field operator

$$F(z)(t) = u_\infty(t), \quad \text{for } t \in [0, 2\pi], \tag{4.6}$$

where $F(z) = S_\infty(z, S_0 u^i(z))$. For a given $z(t)$ one can linearize (4.6) to find an update $z + h$. Linearizing this equation involves the Fréchet derivative of the classical boundary to far field operator, see Section 5 in Colton and Kress [**2**]. The Fréchet derivative of the operator F can be formally calculated in the following way

$$\begin{aligned} F'[z]h = {} & S'_\infty[z, S_0 u^i(z)]h + S_\infty(z, S_0 S'[z, S_0 u^i(z)]h) \\ & + S_\infty(z, S_0(u^{i\prime}[z]h)). \end{aligned} \tag{4.7}$$

The operators on the right-hand side of (4.7) have been defined in subsections 3.1–3.3 so it is possible to build a third iterative method for solving the inverse scattering problem. This approach is related to a method described in [**2**, Section 5].

Conclusions. In this study the problem of reconstructing a planar sound-soft obstacle from knowledge of the far field data for one incoming wave has been considered. Two procedures were proposed based on

the integral equations for the incoming wave and the far field data. Numerical comparisons were carried out between the two approaches for several different types of obstacles, incoming waves and initial guesses. In general, method B produces a good reconstruction in fewer iterations than are required in method A. However, in order to decrease the error level further method A requires fewer steps. Method A usually performs in a way that it moves the initial guess towards the center of the obstacle, then the illuminated region is found and finally the shadow region is reconstructed while method B searches directly for the illuminated part and then locates the shadow region. In addition, with noisy data accurate reconstructions are obtained in relatively few iterations for both methods with slightly better accuracy for Method A.

Acknowledgments. We would like to thank Rainer Kress and Brian Sleeman for the helpful discussions and valuable suggestions to improve this paper. The second author would also like to thank the Institute for Numerical and Applied Mathematics in Göttingen for their hospitality and support.

REFERENCES

1. D. Colton and A. Kirsch, *A simple method for solving inverse scattering problems in the resonance region*, Inverse Problems **12** (1996), 383–393.

2. D. Colton and R. Kress, *Inverse acoustic and electromagnetic scattering*, Springer-Verlag, Berlin, 1998.

3. D. Colton and P. Monk, *A novel method for solving the inverse scattering problem for time-harmonic acoustic waves in the resonance region*, SIAM J. Appl. Math. **45** (1985), 1039–1053.

4. ———, *A novel method for solving the inverse scattering problem for time-harmonic acoustic waves in the resonance region* II, SIAM J. Appl. Math. **46** (1986), 506–523.

5. D. Colton and B.D. Sleeman, *Uniqueness theorems for the inverse problem of acoustic scattering*, IMA J. Appl. Math. **31** (1983), 253–259.

6. J. Fan and J. Pan, *Inexact Levenberg-Marquardt method for nonlinear equations*, Discrete Continuous Dynamic Systems **4** (2004), 1223–1232.

7. J. Hadamard, *Lectures on Cauchy's problem in linear partial differential equations*, Yale University Press, New Haven, 1923.

8. M. Ikehata, *Reconstruction of an obstacle from the scattering amplitude at a fixed frequency*, Inverse Problems. **14** (1998), 949–954.

9. O. Ivanyshyn and R. Kress, *Nonlinear integral equations in inverse obstacle*

scattering, in *Mathematical methods in scattering theory and biomedical engineering*, Fotiatis and Massalas, eds., World Scientific, Singapore, 2006.

10. T. Johansson and B.D. Sleeman, *Reconstruction of an acoustically sound-soft obstacle from one incident field and the far field pattern*, IMA J. Appl. Math. **72**, (2007), 96–112.

11. A. Kirsch, *Numerical algorithms in inverse scattering theory*, in *Ordinary and partial differential equations*, B.D. Sleeman and R.J. Jarvis, eds., Pitman, Boston, 1993.

12. ———, *Characterization of the shape of a scattering obstacle using spectral data of the far field operator*, Inverse Problems **14** (1998), 1489–1512.

13. A. Kirsch, R. Kress, P. Monk and A. Zinn, *Two methods for solving the inverse acoustic scattering problem*, Inverse Problems **4** (1988), 749–770.

14. R. Kress and W. Rundell, *Inverse scattering for shape and impedance*, Inverse Problems **17** (2001), 1075–1085.

15. R. Kress and P. Serranho, *A hybrid method for two-dimensional crack reconstruction*, Inverse Problems **21** (2005), 773–784.

16. R. Kress and I. Sloan, *On the numerical solution of a logarithmic integral equation of the first kind for the Helmholtz equation*, Numer. Math. **66** (1993), 199–214.

17. R. Potthast, *Fréchet differentiability of boundary integral operators in inverse acoustic scattering*, Inverse Problems **10** (1994), 431–447.

18. ———, *A fast new method to solve inverse scattering problems*, Inverse Problems **12** (1996), 731–742.

19. ———, *On the convergence of a new Newton-type method in inverse scattering*, Inverse Problems **17** (2001), 1419–1434.

20. B.D. Sleeman, *The inverse problem of acoustic scattering*, Appl. Math. Institute Technical Report No. 114 A, University of Delaware, Newark, 1981.

Institute for Numerical and Applied Mathematics, Georg-August University of Göttingen, Lotzestr. 16–18, Göttingen, Germany
Email address: ivanyshy@math.uni-goettingen.de

School of Mathematics, University of Birmingham, Edgbaston, Birmingham B15 2TT, UK
Email address: b.t.johansson@bham.ac.uk